Calorimetric Studies on Antiferromagnetic and Structural Phase Transitions of the Metal-Assembled Complex MnCu(obbz)·5H_2O#

Kaori Asano, Kazuhiro Inoue, Motohiro Nakano,## Yuji Miyazaki, Michio Sorai,*

Keitaro Nakatani,†,### and Olivier Kahn†

Microcalorimetry Research Center, School of Science, Osaka University, Toyonaka, Osaka 560-0043

†Laboratoire des Sciences Moléculaires, Institut de Chimie de la Matière Condenscée de Bordeaux, F-33608 Pessac, France

(Received March 1, 1999)

Heat capacities of the molecule-based antiferromagnet MnCu(obbz)·5H_2O (obbz = oxamidobis(benzoato)) have been measured at temperatures from 0.1 to 300 K by means of adiabatic calorimetry. A phase transition due to three-dimensional antiferromagnetic ordering was observed at 2.18 K, above which a heat capacity hump appeared, arising from the short-range ordering characteristic of a low-dimensional magnet. The enthalpy and entropy gained at the magnetic phase transition were evaluated to be 48.6 J mol^{-1} and 12.1 J K^{-1} mol^{-1}, respectively. This entropy gain is close to the value $R \ln 5$ (= 13.4 J K^{-1} mol^{-1}) expected for the spin-manifold of the $S = 2$ ground state. The heat capacity hump above the magnetic transition temperature is explained well by the $S = 2$ one-dimensional ferromagnetic Heisenberg model with the exchange interaction $J/k_B = 0.75$ K, where k_B is the Boltzmann constant. These results confirm that the present complex behaves as a one-dimensional ferrimagnet, in which strong antiferromagnetic coupling exists between a pair of spins of Mn(II) ($S = 5/2$) and Cu(II) ($S = 1/2$) but the magnetic interaction is very weak between the pairs. A first-order phase transition was also found at 268.4 K. This transition may arise from orientational order–disorder mechanism of the crystalline water molecules in the complex.

Molecule-based magnets have provided us with both theoretically and experimentally interesting research subjects for the past decade. Many strategies for preparing molecule-based ferromagnets have been developed. Miller et al.[1—5] first synthesized the molecule-based ferromagnet [Fe(Me_5cp)$_2$][TCNE] (Me_5cp = pentamethylcyclopentadienyl, TCNE = tetracyanoethylene) with $T_c = 4.8$ K on the basis of a charge-transfer mechanism. Kahn et al.[6,7] synthesized a ferromagnetic mixed-metal complex MnCu(pbaOH)(H_2O)$_3$ (pbaOH = 2-hydroxy-1,3-propanediylbis(oxamato)) with $T_c = 4.6$ K. Gatteschi et al.[8—10] synthesized Mn(hfa)$_2$(NITiPr) (hfa = hexafluoroacetylacetonato, NITiPr = 2-isopropyl-4,4,5,5-tetramethyl-4,5-dihydro-1*H*-imidazolyl-1-oxyl-3-oxide) with $T_c = 7.8$ K by the use of free radicals as the ligands of transition metal.

Kahn et al.[11] reported a novel molecule-based ferromagnet MnCu(obbz)·H_2O (obbz = oxamidobis(benzoato)) with high T_c (= 14 K), which is obtained by partial dehydration of the molecule-based antiferromagnet MnCu(obbz)·5H_2O. It has been shown by powder X-ray diffraction patterns and XANES and EXAFS spectra at both Mn and Cu edges for MnCu(obbz)·5H_2O and MnCu(obbz)·H_2O[12] that these complexes have very similar structures and that Mn(II) and Cu(II) ions are in octahedral and elongated tetragonal surroundings, respectively. These structural results imply that Mn(II) and Cu(II) ions are bridged alternately by oxamido and carboxylato groups to form one-dimensional chains, which are two- or three-dimensionally connected through Mn(II)–O(oxamido) bonds. In MnCu(obbz)·5H_2O, only one water molecule is coordinated to Mn(II) ion and the remaining four water molecules are non-coordinated, coinciding with the easy dehydration. Magnetic measurements[12] indicate that the $\chi_M T$ versus T plot for MnCu(obbz)·5H_2O has a minimum around 40 K characteristic of alternating bimetallic or ferrimagnetic chains coupled antiferromagnetically and shows a sharp maximum due to three-dimensional antiferromagnetic ordering at 2.3 K, where χ_M is the molar magnetic susceptibility per MnCu unit and T is temperature. The $\chi_M T$ versus T plot for MnCu(obbz)·H_2O diverges in approaching the critical temperature $T_c = 14$ K, below which MnCu(obbz)·H_2O exhibits a spontaneous magnetization. Both complexes show saturation magnetizations corresponding to a $S = 2$ resulting spin per MnCu unit under magnetic field.

In the present work, we have measured heat capacities of the molecule-based antiferromagnet MnCu(obbz)·5H_2O. Adiabatic heat capacity calorimetry is one of the powerful

Contribution No. 166 from the Microcalorimetry Research Center.

Present address: Department of Molecular Chemistry, Graduate School of Engineering, Osaka University, Toyonaka, Osaka 560-0043, Japan.

Present address: Laboratoire de Photophysique et Photochimie Moleculaires et Macromoleculaires, Ecole Normale Superieure de Cachan, 94235 Cachan, France.

methods for elucidating the thermal properties associated with a change in magnetic properties of substances. We observed not only the antiferromagnetic phase transition predicted by the magnetic measurement[12] but also a structural phase transition. We report in this paper precise and accurate thermodynamic quantities associated with these phase transitions and discuss the mechanism of the phase transitions.

Experimental

Sample Preparation. MnCu(obbz)·5H_2O was synthesized in two batches according to a method described elsewhere.[12] The results of elemental analysis for the two obtained batches of the complex are as follows. Calcd for MnCu(obbz)·5H_2O ($C_{16}H_{18}N_2O_{11}CuMn$): C, 36.07; H, 3.41; N, 5.26%. Found: C, 36.00; H, 3.49; N, 5.16% for batch 1 and C, 35.87; H, 3.41; N, 5.18% for batch 2.

We carried out thermogravimetry (TG) for 2.440 mg of the sample from batch 2 with a thermogravimetric analyzer (Perkin–Elmer, TGA7) from room temperature to 500 °C at the heating rate of 10 K min^{-1} to confirm the amount of crystalline water contained in the sample. The result of this TG measurement is shown in Fig. 1. The first weight loss of 0.356 mg occurred between room temperature and 90 °C. The sample weight was kept constant between 90 and 350 °C. The second weight loss began above 350 °C. The constant weight region corresponds to MnCu(obbz)·H_2O[12] and the second weight loss region indicates decomposition of the sample. Since, at the first weight loss, 4.3 mol of the crystalline water was removed from the sample, the amount of the crystalline water contained in the virginal sample was assumed to be 5.3 mol. Actually, the results of elemental analyses for both the batches of the sample agreed well with MnCu(obbz)·5.3H_2O (C, 35.71; H, 3.48; N, 5.20%).

Heat Capacity Measurement. Heat capacity measurement of MnCu(obbz)·5H_2O was performed with two types of adiabatic calorimeters, depending on the optimum temperature range. For the measurement between 0.1 and 17 K a very-low-temperature adiabatic calorimeter workable with a $^3He/^4He$ dilution refrigerator[13] was used. The sample from batch 1 (6.2286 g) was loaded into a gold-plated copper cell together with 4.7780 g of Silicone oil (Toshiba Silicone, TSF433) to aid in the thermal conduction between the sample and the cell. The measurement for 5.6698 g of the batch 2 sample was carried out from 11 to 300 K with a low-temperature adiabatic calorimeter.[14] The sample was loaded into a gold-plated copper cell together with 590 Torr of ^4He gas as a heat exchange medium (1 Torr = 133.322 Pa). Buoyancy correction for the mass of sample was made by assuming a density of 1.8 g cm^{-3}.[12] It should be remarked here that the heat capacity data given in tables and figures of the present paper are the values corrected to the pentahydrate on the assumption of additivity between the heat capacities of MnCu(obbz)·5H_2O and the excess 0.3 mol of H_2O.

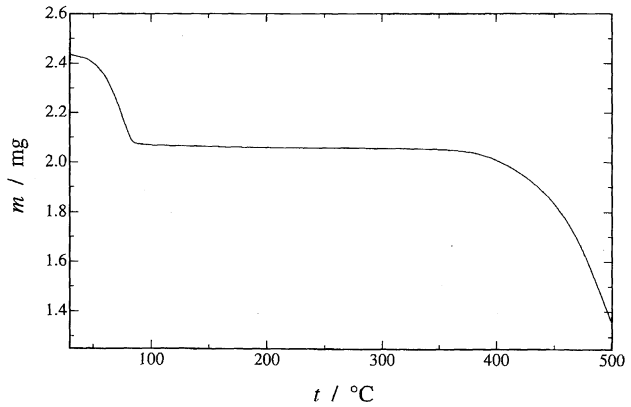

Fig. 1. Thermogravimetry for MnCu(obbz)·5H_2O from batch 2. Mass and Celsius temperature are denoted by *m* and *t*, respectively.

Infrared and Raman Spectroscopy. Infrared (IR) spectra of MnCu(obbz)·5H_2O were recorded for Nujol mulls at 100 and 200 K and room temperature in the range of 400—4000 cm^{-1} with an infrared spectrophotometer (Japan Spectroscopic Co., Ltd., Model DS-402G). Raman spectra of the sample were recorded at 100 and 200 K and room temperature in the range of 500—1800 cm^{-1} with a laser Raman spectrophotometer (Japan Spectroscopic Co., Ltd., Model R-800) using the 632.8 nm line from a He–Ne source for excitation.

Powder X-Ray Diffraction. Powder X-ray diffraction patterns of MnCu(obbz)·5H_2O were taken at 100, 200, and 300 K with a diffractometer (Rigaku Denki Co., Ltd., Model Rad-Roc). The region of reflection angle was $3° < 2\theta < 90°$ and the scanning speed was 3 ° min^{-1}.

Results and Discussion

Heat Capacity. The molar heat capacities of MnCu(obbz)·5H_2O are tabulated in Table 1 and plotted in Fig. 2. To demonstrate the reproducibility of the measurements, heat capacities in the 1—3.5 K range determined in series 1, 3, 4, 5, and 6 are plotted in Fig. 3. Two heat capacity peaks due to phase transitions were found at 2.18 and 268.4 K. The peak at 2.18 K corresponds to the antiferromagnetic phase transition T_N, because the transition temperature agrees well with the maximum temperature 2.3 K of the $\chi_M T$ versus T plot.[12] As discussed later, a heat capacity hump was also observed above the transition temperature. This heat-capacity anomaly is due to the short-range order effect of the spin alignment characteristic of low-dimensional magnets.

The peak at 268.4 K is regarded as a non-magnetic phase transition, because there is no magnetic anomaly around this temperature region.[12] The inverse of the cooling rate of the calorimeter cell containing sample reflects the heat capacity of sample at cooling direction. Figure 4 shows the inverse of the cooling rate against temperature recorded by monitoring the cooling rate of the calorimeter cell. Two peaks were found: a sharp peak at 262 K and a broad one centered at 257 K. If one judges from the peak area, the sharp peak corresponds to freezing of the water occluded in the complex and the broad peak is due to the intrinsic phase transition. This means that the synthesized sample contained 0.3 mol of extra free water. This fact is consistent with the results of the elemental analysis and the thermogravimetry described above. Consequently, we corrected the observed heat capacity data to the molar heat capacities of MnCu(obbz)·5H_2O by assuming additivity between the heat capacities of MnCu(obbz)·5H_2O and H_2O.[15,16] Since the phase transition occuring at 268.4 K was remarkably supercooled at 257 K on the cooling experiment, this phase transition has a first-order nature.

Table 1. Molar Heat Capacities of MnCu(obbz)·5H_2O (M = 532.81 g mol^{-1})
Data in Series 1—6 and Series 7—11 were collected by use of different adiabatic calorimeters.

T/K	C_p/J K^{-1} mol^{-1}	T/K	C_p/J K^{-1} mol^{-1}	T/K	C_p/J K^{-1} mol^{-1}	T/K	C_p/J K^{-1} mol^{-1}
Series 1		1.432	3.592	2.859	4.639	4.221	4.533
0.157	0.601	1.493	3.811	2.932	4.590	4.438	4.659
0.174	0.605	1.558	4.073	3.023	4.546	4.666	4.688
0.210	0.691	1.624	4.285	3.114	4.563	6.264	5.199
0.244	0.685	1.691	4.540	3.208	4.494	6.888	5.317
0.286	0.716	1.761	4.549	3.303	4.579	7.201	5.527
0.322	0.778	1.842	5.357	3.551	4.549	7.849	6.113
0.356	0.839	1.931	5.689	3.691	4.526	8.690	6.658
0.389	0.878	2.020	6.443	3.842	4.562	9.610	7.961
0.418	0.952	2.101	7.438	4.006	4.571		
0.444	1.045	2.182	8.194	5.280	4.851	Series 7	
0.469	1.073	2.285	7.003	5.524	4.878	78.64	184.7
0.484	1.101	2.395	5.716	6.015	5.068	80.63	189.4
0.513	1.179	2.499	5.486	6.277	5.314	82.56	194.0
0.541	1.260	2.596	5.047	7.410	5.838	84.45	198.5
0.567	1.317	2.699	4.989	7.704	5.975	86.30	202.8
0.590	1.367	2.804	5.010	8.043	6.232	88.10	206.9
0.614	1.367	2.917	4.818	8.398	6.594	89.88	211.0
0.700	1.578	3.034	4.659	8.769	6.737	91.62	214.8
0.726	1.665	3.171	4.463	9.151	7.106	93.34	218.6
0.750	1.748	3.325	4.220	9.544	7.575	95.02	222.2
0.770	1.776	3.475	4.229	9.952	8.185	96.68	225.8
0.791	1.784	3.626	4.360	10.38	8.730	98.31	229.3
0.813	1.866	3.790	4.302	10.82	9.369	99.93	232.5
0.836	1.926	3.961	4.336	11.28	10.21	101.52	236.0
0.876	1.973	4.136	4.365	11.76	10.82	103.09	239.3
0.912	2.095	4.314	4.432	12.25	11.76	104.64	242.3
0.947	2.186	4.501	4.536	12.76	13.01	106.37	245.9
0.977	2.302	4.692	4.701	13.30	13.45	108.26	249.6
1.003	2.331	4.888	4.738	14.42	15.96	110.13	253.5
1.025	2.374			15.02	17.21	111.98	257.0
1.047	2.490	Series 4		15.64	18.59	113.81	261.0
1.073	2.534	1.100	2.548	16.27	19.61	115.61	264.8
1.098	2.575	1.174	2.808	16.93	21.64	117.40	268.5
1.120	2.635	1.244	3.077			119.17	272.1
		1.324	3.236	Series 5		120.91	275.7
Series 2		1.408	3.479	1.828	5.005	122.65	279.5
0.164	0.617	1.495	3.685	1.892	5.512	124.36	283.0
0.180	0.644	1.580	4.114	1.967	6.067	126.06	286.3
0.196	0.622	1.663	4.485	2.047	6.741	127.75	289.8
0.213	0.648	1.755	4.628	2.127	7.803	129.42	293.2
0.231	0.626	1.838	5.272	2.215	7.982	131.08	296.7
0.247	0.638	1.916	5.661	2.289	6.786	132.72	300.0
0.263	0.663	1.987	6.140	2.346	5.961	134.36	303.2
0.280	0.707	2.053	6.644	2.760	4.798	135.98	306.5
0.299	0.764	2.119	7.339	3.208	4.547	137.59	309.5
0.319	0.789	2.188	7.844			139.19	313.0
0.338	0.803	2.255	7.308	Series 6			
0.354	0.861	2.311	6.580	2.505	5.191	Series 8	
0.368	0.864	2.362	5.893	2.645	4.787	11.52	10.16
0.380	0.923	2.412	5.541	2.788	4.657	12.25	11.53
		2.460	5.503	2.942	4.511	12.97	13.16
Series 3		2.514	5.031	3.102	4.424	13.67	14.57
1.177	2.928	2.568	4.889	3.267	4.393	14.37	15.95
1.200	3.078	2.622	4.940	3.438	4.440	15.06	17.42
1.250	3.075	2.685	4.803	3.620	4.511	15.76	18.68
1.309	3.307	2.744	4.683	3.813	4.482	16.45	20.06
1.369	3.424	2.801	4.620	4.012	4.525	17.15	21.48

Table 1. (Continued)

T/K	C_p/J K^{-1} mol^{-1}	T/K	C_p/J K^{-1} mol^{-1}	T/K	C_p/J K^{-1} mol^{-1}	T/K	C_p/J K^{-1} mol^{-1}
17.85	22.89	219.61	473.8	262.27	790.7	56.51	129.7
18.60	24.57	221.54	478.0	263.88	916.9	57.96	133.6
19.37	26.16	223.46	482.4	265.35	1115	59.65	138.0
20.08	27.92	225.37	486.7	266.69	1355	61.62	143.1
20.74	29.45	227.27	491.2	267.91	1506	63.68	148.5
21.42	31.17	229.16	495.9	269.09	1502	65.66	153.5
22.11	32.91	231.05	500.6	270.33	1306	67.56	158.3
22.85	34.89	232.93	506.1	271.71	986.1	69.40	163.0
23.65	37.07	234.86	512.0	273.31	730.1	71.18	167.4
24.39	39.11	236.84	517.7	275.07	634.7	72.91	171.6
25.11	41.11	238.81	524.7	276.88	610.5	74.59	175.7
		240.77	531.0	278.72	608.8	76.50	180.3
Series 9		242.72	538.1	280.55	610.1	78.62	185.4
137.83	311.0	244.66	546.0	282.38	613.8	80.68	190.3
138.92	313.4	246.60	554.5	284.20	617.2	82.49	194.5
140.22	315.6	248.52	563.9	286.02	621.3	84.06	198.4
141.51	318.3	250.43	574.6	287.84	625.0	85.61	201.8
142.79	320.6	252.32	587.2	289.65	628.6	87.13	205.2
144.07	323.0	254.19	602.7	291.45	631.8	88.62	208.6
145.34	325.2	256.03	625.6	293.24	635.8		
147.08	329.1	257.85	654.5	295.14	641.8		
149.29	333.4	259.63	695.3	297.13	645.2		
151.48	337.7	261.35	756.6	299.12	649.3		
153.66	342.0	263.00	826.2				
155.82	346.2	264.56	1010	Series 11			
157.96	350.4	265.96	1228	18.97	24.41		
160.09	354.4	267.23	1428	19.71	26.23		
162.20	358.7	268.42	1513	20.39	27.80		
164.30	362.9	269.61	1417	21.14	29.72		
166.20	366.0	270.89	1179	21.90	31.63		
167.90	369.5	272.36	841.7	22.68	33.69		
169.59	373.0	274.03	669.9	23.59	36.13		
171.28	376.1	275.81	615.4	24.59	38.88		
172.96	379.5	277.62	608.2	25.56	41.57		
174.62	382.5	279.43	608.9	26.53	44.21		
176.28	386.1	281.24	611.6	27.55	47.12		
178.01	389.3	283.05	615.4	28.60	50.11		
179.80	392.8	284.85	617.8	29.67	53.15		
181.58	396.3	286.64	621.9	30.82	56.50		
183.36	399.8	288.44	626.1	32.68	62.84		
185.13	403.3	290.22	629.7	33.85	65.73		
186.88	406.8	292.00	633.4	35.13	68.85		
188.63	410.3	293.88	637.9	36.42	72.95		
190.38	414.0	295.87	643.4	37.68	76.65		
192.11	417.2	297.86	647.1	38.87	80.00		
193.84	420.8	299.85	651.1	39.99	83.22		
195.56	424.2			41.05	86.33		
197.27	427.3	Series 10		42.06	89.29		
198.98	430.9	241.78	530.6	43.04	92.16		
200.67	434.4	243.73	538.9	43.97	94.82		
202.36	437.7	245.67	547.7	44.87	97.36		
204.05	441.1	247.60	557.5	45.94	100.5		
205.88	444.5	249.51	567.6	47.25	104.2		
207.87	448.5	251.41	579.6	48.55	107.7		
209.85	452.6	253.30	592.6	49.80	111.3		
211.82	456.8	255.17	609.3	51.04	114.7		
213.78	460.9	257.01	630.9	52.30	118.1		
215.73	464.9	258.82	611.2	53.68	121.9		
217.68	469.2	260.58	714.0	55.12	125.9		

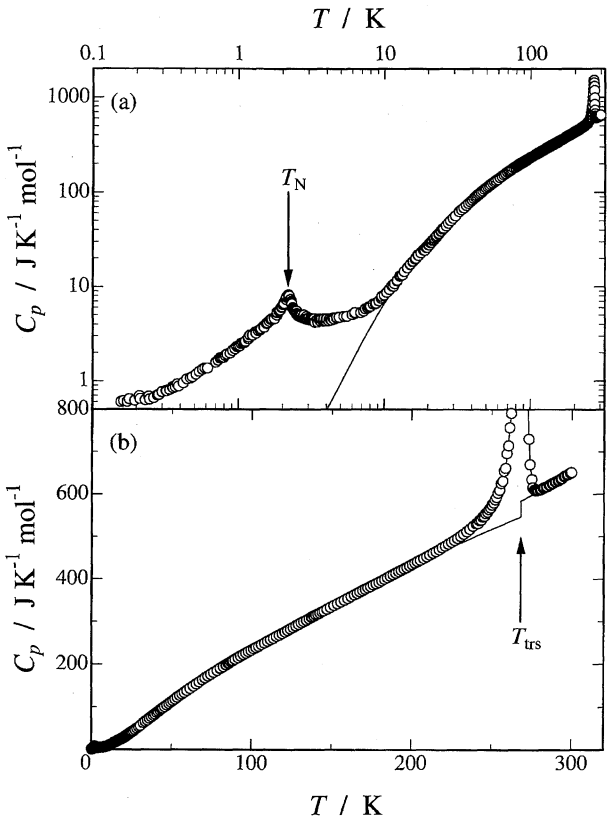

Fig. 2. Molar heat capacities of MnCu(obbz)·5H_2O on (a) logarithmic and (b) normal scales. Solid curves indicate the normal heat capacities.

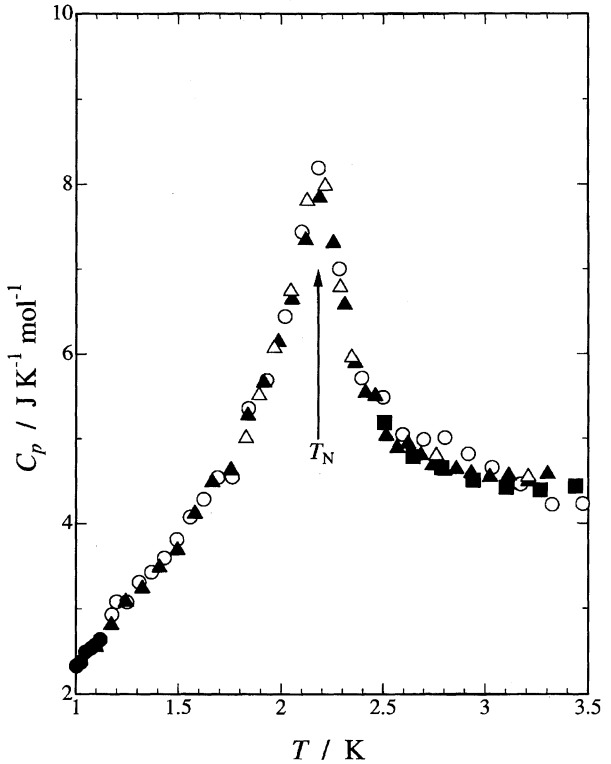

Fig. 3. Molar heat capacities of MnCu(obbz)·5H_2O in the vicinity of the magnetic phase transition. ●: Series 1, ○: Series 2, ▲: Series 4, △: Series 5, ■: Series 6.

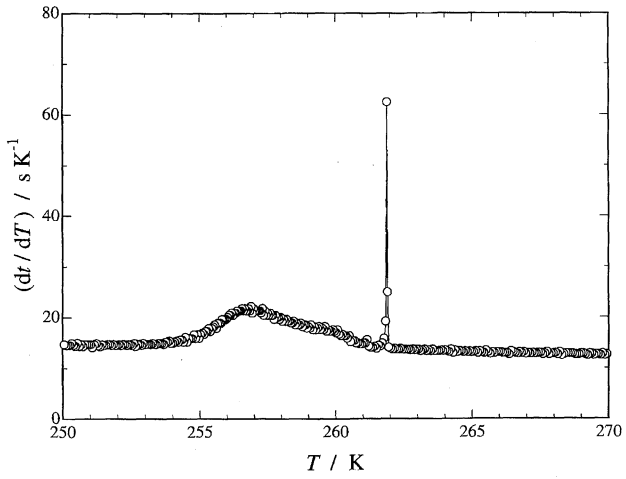

Fig. 4. Plots of the inverse of cooling rate versus temperature for the calorimetric cell containing MnCu(obbz)·5H_2O.

Determination of Normal and Excess Heat Capacities. It is necessary to estimate the normal heat capacities of MnCu(obbz)·5H_2O for determination of the excess heat capacities due to phase transitions. We adapted an effective frequency distribution method[17] to determine the normal heat capacities below the structural phase transition temperature. Since this complex consists of 49 atoms for a formula unit, the number of degrees of freedom is 147, among which the contribution from intramolecular vibrations is 141. We could assign totally 91 normal mode frequencies of intramolecular vibration on the basis of experimental IR and Raman spectra and the literature values for the constituent moieties.[18—20] The contribution from these 91 optical modes to the normal heat capacity was calculated according to the Einstein model. The remaining 50 optical modes, 6 acoustic modes for lattice vibrations, and the (C_p-C_V) correction were effectively included in a frequency distribution spectrum, which was determined by non-linear least squares fitting in the temperature range from 9 to 180 K, where the influence of the phase transitions is very small. Since the heat capacities far above the magnetic transition temperature are usually assumed to include a term proportional to T^{-2}, we took into account this term for the fitting. The normal heat capacities above the structural transition temperature were determined by simply assuming a straight line and fitting it to the heat capacities above 280 K.

The normal heat capacities thus obtained are drawn in Fig. 2 by solid curves. The proportional coefficient of the T^{-2} term was determined to be 155 J K mol^{-1}. The excess heat capacities were derived by subtracting the normal heat capacities from the experimental values. Figure 5 shows the excess heat capacities ΔC_p as a function of temperature. It is easily recognized that a heat capacity hump centered around 4 K obviously exists due to short-range ordering of the spins above the magnetic transition temperature.

Transition Enthalpies and Entropies. The enthalpy and entropy changes due to the two phase transitions can be evaluated from the excess heat capacities. The magnetic enthalpy and entropy due to the antiferromagnetic phase tran-

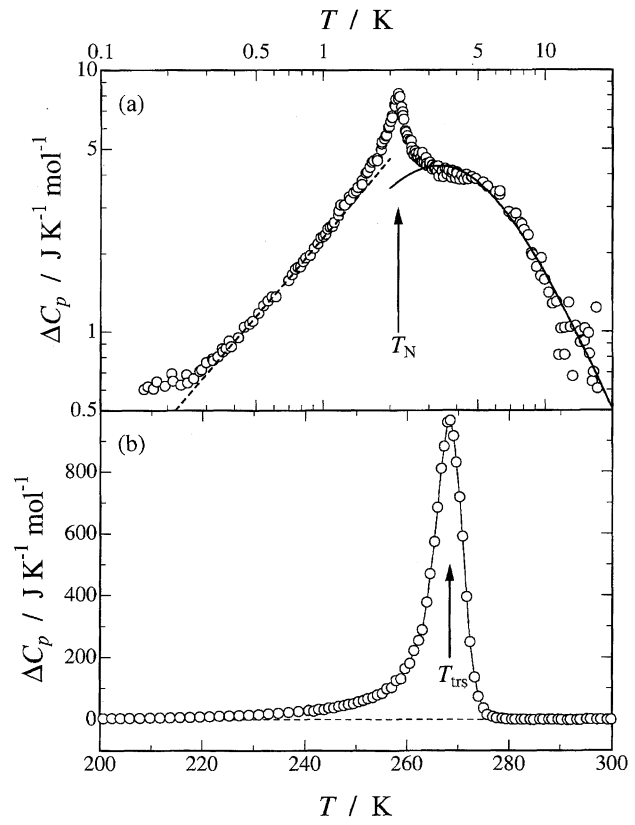

Fig. 5. Excess heat capacities of $MnCu(obbz)\cdot 5H_2O$ around (a) the antiferromagnetic phase transition temperature and (b) the structural phase transition temperature. Solid curve in (a) indicates the theoretical heat capacity curve estimated by the high-temperature series expansion for $S = 2$ one-dimensional ferromagnetic Heisenberg model with $J/k_B = 0.75$ K. Broken line in (a) shows the heat capacity derived from the spin wave theory for one-dimensional antiferromagnets. Solid line in (b) is only eye guide.

sition were calculated as follows. The enthalpy and entropy gained between 0.4 and 18.6 K were calculated by the direct integration of the excess heat capacities with respect to T and $\ln T$, respectively. The enthalpy and entropy gains from 0 to 0.4 K were estimated on the basis of the spin wave theory, which will be discussed later. The contributions from 18.6 K to infinite temperature were calculated by integrating the T^{-2} term described above with respect to T and $\ln T$, respectively. The entire magnetic enthalpy and entropy thus evaluated amounted to 48.6 J mol^{-1} and 12.1 J K^{-1} mol^{-1}, respectively.

On the other hand, the transition enthalpy and entropy for the phase transition at 268.4 K were evaluated by integrating the excess heat capacities from 175 to 280 K with respect to T and $\ln T$. The transition enthalpy and entropy thus determined were 7.17±0.01 kJ mol^{-1} and 27.6±0.1 J K^{-1} mol^{-1}, respectively, where the enthalpy and entropy of fusion for 0.3 mol of the excess H_2O[15] have been subtracted.

Mechanism of the Antiferromagnetic Phase Transition. As stated in the Introduction, $MnCu(obbz)\cdot 5H_2O$ has a two- or three-dimensional network structure formed by linear chains, in which Mn(II) and Cu(II) ions are alternately bridged by two different kinds of groups: oxamido and calboxylato.[12] The magnetic susceptibility measurement[12] indicated that this complex can be regarded as a one-dimensional ferrimagnet composed of two different spins $S = 5/2$ for Mn(II) and $S = 1/2$ for Cu(II) above the antiferromagnetic transition temperature. The magnetic structure of this one-dimensional ferrimagnetic chain is schematically drawn in Fig. 6(a). The exchange interaction parameters for the oxamido and carboxylato bridges between Mn(II) and Cu(II) have been determined to be $J_1 = -29$ cm^{-1} and $J_2 = -5$ cm^{-1}, respectively. This suggests that the one-dimensional ferrimagnetic chain can be regarded as a one-dimensional pseudo ferromagnetic chain made up of $S = 2$ resultant spins arising from pairing between the spins of Mn(II) and Cu(II). This is caused by the fact that the exchange interaction for the oxamido bridge is much stronger than that for the carboxylato bridge.

The total entropy gain theoretically expected for the spin multiplicity of Mn(II) and Cu(II) amounts to $R \ln(6\times 2)$ (= 20.7 J K^{-1} mol^{-1}). However, since this ferrimagnetic chain can be regarded as an $S = 2$ pseudo-ferromagnetic linear chain for the reason described above, only $R \ln 5$ (= 13.4 J K^{-1} mol^{-1}) contributes to the entropy at low temperatures. Although the experimental entropy gain 12.1 J K^{-1} mol^{-1} is slightly smaller than this value, we conclude that they agree well enough and that the pseudo-ferromagnetic chain model is a good approximation when the uncertainty involved in

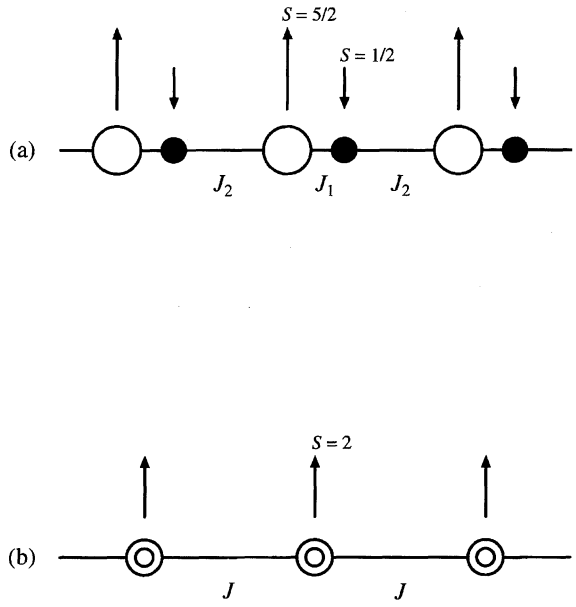

Fig. 6. (a) Schematic magnetic structure of the one-dimensional ferrimagnetic chain in $MnCu(obbz)\cdot 5H_2O$. Open and filled circles stand for Mn(II) and Cu(II) ions, respectively. Long and short arrows indicate spin 5/2 and 1/2, respectively. Antiferromagnetic interaction J_1 is much stronger than J_2. (b) One-dimensional ferromagnetic chain consisting of the resultant $S = 2$ spins expected for the antiferromagnetically strongly couples Mn(II) and Cu(II) spin pair. Double circle stands for the Mn(II)–Cu(II) pair. The definition of the exchange parameter J is given in the text.

the estimate of the normal heat capacity curve is taken into account.

The remaining entropy of $R\ln(12/5)$ (= 7.3 J K^{-1} mol^{-1}) would be acquired at higher temperatures by thermal excitation to the $S = 3$ spin level. One of the ways to see this entropy acquisition is to approximate the ferrimagnetic linear chain by an array of strongly coupled Mn(II) and Cu(II) pairs, and to neglect the magnetic interaction between the pairs. We shall assume antiferromagnetically coupled pairs with $J_1 = -29$ cm^{-1} ($J_1/k_B = -42$ K),[12] where k_B denotes the Boltzmann constant. The spin energy level scheme of such an isolated pair can be easily derived on the basis of the vector model.[21] In contrast with Ref. 12, in the following we will adopt the form $\boldsymbol{H} = -2J_1'\boldsymbol{S}_{Mn}\cdot\boldsymbol{S}_{Cu}$ for the spin Hamiltonian between the spins $\boldsymbol{S}_{Mn}$ and $\boldsymbol{S}_{Cu}$ of Mn(II) and Cu(II).

$$\begin{aligned}\boldsymbol{H} &= -2J_1'\boldsymbol{S}_{Mn}\cdot\boldsymbol{S}_{Cu}\\ &= -J_1'\boldsymbol{S}^2 + J_1'\left(\boldsymbol{S}_{Mn}^2 + \boldsymbol{S}_{Cu}^2\right),\end{aligned} \tag{1}$$

where $J_1 = 2J_1'$ and $\boldsymbol{S} = \boldsymbol{S}_{Mn}+\boldsymbol{S}_{Cu}$. The eigenvalue E is expressed by the following equation:

$$\begin{aligned}E &= -J_1'S(S+1) + J_1'S_{Mn}(S_{Mn}+1) + J_1'S_{Cu}(S_{Cu}+1)\\ &= -J_1'S(S+1) + (19/2)J_1'.\end{aligned} \tag{2}$$

Here $S_{Mn} = 5/2$ and $S_{Cu} = 1/2$.

The energy scheme thus determined consists of the five-fold degenerate ground level with $S = 2$ and the seven-fold degenerate excited level with $S = 3$. From Eq. 2, the energy separation between these two levels is $-6J_1'$. The magnetic heat capacity arising from this two-level scheme corresponds to a Schottky anomaly. As shown in Fig. 7, this Schottky anomaly brings about a very broad heat capacity peak centered around ca. 50 K when $J_1'/k_B = -21$ K (or $J_1/k_B = -42$ K). Since the magnitude of this anomaly is very small in comparison to the total heat capacity and furthermore the anomaly is very broad, it is difficult (or impossible) to separate it from the experimental heat capacity.

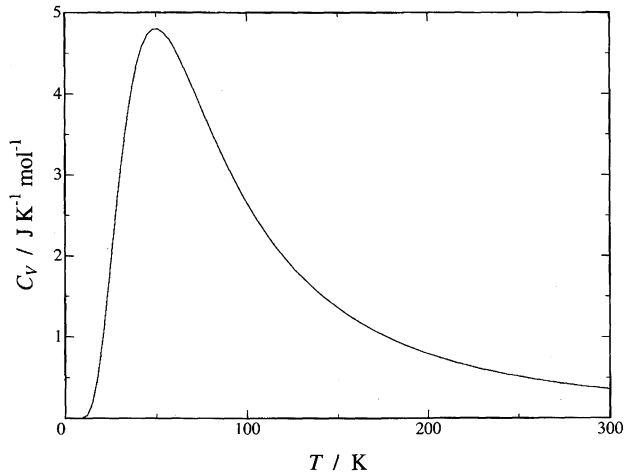

Fig. 7. Schottky heat capacity curve of a two-energy-level system with the degeneracy ratio of 5 : 7 and the energy separation of $126k_B$ K (= $-6J_1'$).

In order to interpret the excess heat capacity due to the short-range order appearing above T_N, we approximated the ferrimagnetic linear chain consisting of the strongly coupled spin-pair of $S_{Mn} = 5/2$ and $S_{Cu} = 1/2$ shown in Fig. 6(a) by a ferromagnetic chain consisting of the resultant $S = 2$ spins depicted in Fig. 6(b). As shown in Fig. 5(a), good agreement was obtained between the observed and the calculated values on the basis of the theoretical treatment[22] when the exchange interaction parameter between the spin pairs is $J/k_B = 0.75$ K, where J is defined as $-2J\boldsymbol{S}_{pair}(\boldsymbol{i})\cdot\boldsymbol{S}_{pair}(\boldsymbol{i}+\boldsymbol{1})$. This agreement may arise from the fact that the exchange interaction along the chain is characterized by the strong alternation. The present ferrimagnetic chain is represented by the spin Hamiltonian:

$$\boldsymbol{H}_{chain} = -2\sum_i[J_1'\boldsymbol{S}_{Mn}(\boldsymbol{i})\cdot\boldsymbol{S}_{Cu}(\boldsymbol{i}) + J_2'\boldsymbol{S}_{Cu}(\boldsymbol{i})\cdot\boldsymbol{S}_{Mn}(\boldsymbol{i}+\boldsymbol{1})]. \tag{3}$$

Because of the strong alternation in a chain, J_1 (= $2J_1'$) $\gg J_2$ (= $2J_2'$), one can assume that each single-ion spin is proportional to the resultant spin, $\boldsymbol{S}(\boldsymbol{i}) = \boldsymbol{S}_{Mn}(\boldsymbol{i})+\boldsymbol{S}_{Cu}(\boldsymbol{i})$, coupled by J_1',

$$\boldsymbol{S}_{Mn}(\boldsymbol{i}) = a\boldsymbol{S}(\boldsymbol{i}), \tag{4a}$$

$$\boldsymbol{S}_{Cu}(\boldsymbol{i}) = b\boldsymbol{S}(\boldsymbol{i}), \tag{4b}$$

where the vector projection coefficients a and b are given by[23]

$$\begin{aligned}a &= [\boldsymbol{S}(\boldsymbol{i})^2 + \boldsymbol{S}_{Mn}(\boldsymbol{i})^2 - \boldsymbol{S}_{Cu}(\boldsymbol{i})^2]/2\boldsymbol{S}(\boldsymbol{i})^2\\ &= [S(S+1) + S_{Mn}(S_{Mn}+1) - S_{Cu}(S_{Cu}+1)]/2S(S+1)\\ &= 7/6,\end{aligned} \tag{5a}$$

$$\begin{aligned}b &= [\boldsymbol{S}(\boldsymbol{i})^2 + \boldsymbol{S}_{Cu}(\boldsymbol{i})^2 - \boldsymbol{S}_{Mn}(\boldsymbol{i})^2]/2\boldsymbol{S}(\boldsymbol{i})^2\\ &= [S(S+1) + S_{Cu}(S_{Cu}+1) - S_{Mn}(S_{Mn}+1)]/2S(S+1)\\ &= -1/6.\end{aligned} \tag{5b}$$

Hence in this vector coupling scheme, the spin Hamiltonian for the chain is written as follows:

$$\boldsymbol{H}_{chain} = \sum_i \boldsymbol{H}_{pair}(\boldsymbol{i}) - 2abJ_2'\sum_i \boldsymbol{S}(\boldsymbol{i})\cdot\boldsymbol{S}(\boldsymbol{i}+\boldsymbol{1}). \tag{6}$$

The first term stands for the summation of the spin-pair Hamiltonian given by Eq. 1, and the second term corresponds to the interpair exchange interaction with J (= $abJ_2' = abJ_2/2$). By substituting $a = 7/6$, $b = -1/6$, and $J_2/k_B = -7.2$ K,[12] the exchange parameter is estimated to be $J/k_B = 0.70$ K. This value is close to the present calorimetric result $J/k_B = 0.75$ K.

Spin wave theory is a good approximation for description of the low-temperature magnetic properties of substances, in the same sense as the lattice heat capacity at low temperatures is well approximated by the Debye theory. The low-temperature heat capacity C_{SW} due to the spin wave excitation can be given by the formula.[24]

$$C_{SW} \propto T^{d/n}, \tag{7}$$

where d is the dimensionality and n is defined as the exponent in the dispersion relation: $n = 1$ for antiferromagnets and $n = 2$ for ferromagnets. In order to investigate the temperature dependence of the magnetic heat capacities of the sample at low temperatures, we fitted the following equation to the magnetic heat capacities between 0.4 and 1 K

$$\Delta C_p = AT^{\alpha} \tag{8}$$

and obtained $\alpha = 0.996 \approx 1$ and $A = 2.29\ \mathrm{J\,K^{-2}\,mol^{-1}}$. The spin wave heat capacity thus obtained is shown in Fig. 5(a) by broken line. This result suggests that in the present complex spins would be arranged in one-dimensional antiferromagnetic order below the magnetic transition temperature T_N. However, since the antiferromagnetic phase transition results from the existence of two- or three-dimensional magnetic interactions, the exponent α should be 2 or 3, that is, two- or three-dimensional antiferromagnetism below T_N. This inconsistency would be attributed to either of the following two reasons: One is that the temperature region from 0.4 to 1 K is not low enough for application of the spin wave theory and the other is that the simple spin wave approximation cannot be applied to a complicated alternating ferrimagnetic system such as the present complex. Although the spin wave heat capacity given by Eq. 7 should be derived on the basis of the dispersion relation of spin wave, no exact dispersion relation has been determined for complicated one-dimensional ferrimagnetic systems, like the present complex, characterized by the alternating spin-spin interactions. Moreover, in the case of low-dimensional magnetic systems,[25] quantum effects[26,27] become significant so that the spin wave theory cannot always describe magnetic behaviors reasonably. Anisotropy inherent in the spin–spin interaction also leads to deviation from the simple spin wave approximation. If one takes these situations into account, the present inconsistency seems to be a natural consequence.

As can be seen in Fig. 5(a), the excess heat capacities of the sample deviate upwards from the spin wave heat capacity line below 0.4 K, as if there were another small thermal anomaly. A plausible origin for this anomaly would be the presence of a small amount of imperfect ferrimagnetic chains which occurred during the sample synthesis.

Mechanism of the Non-Magnetic Phase Transition. The first-order phase transition at 268.4 K is regarded as an order-disorder phase transition because the transition entropy is very large ($\Delta_{trs}S = 27.6 \pm 0.1\ \mathrm{J\,K^{-1}\,mol^{-1}}$). Figure 8 shows the powder X-ray diffraction patterns of MnCu(obbz)·$5H_2O$ at 100, 200, and 300 K. In spite of the first-order phase transition, no remarkable change was observed between the patterns recorded below and above the transition temperature. This fact suggests that the phase transition is not ascribed to a structural change of the ligands forming the ferrimagnetic chains. In the case of MnCu(obbz)·H_2O obtained by partial dehydration of MnCu(obbz)·$5H_2O$, no phase transition was observed.[28] Therefore, it turns out that the phase transition found in MnCu(obbz)·$5H_2O$ is closely associated with the crystalline water molecules. Since the experimental transition entropy is very close to $5R\ln 2 = 28.8\ \mathrm{J\,K^{-1}\,mol^{-1}}$, we can conclude that five crystalline water molecules in the crystal lattice would undergo orientational disordering between two directions above the transition temperature and settle down in either of the directions below the transition temperature.

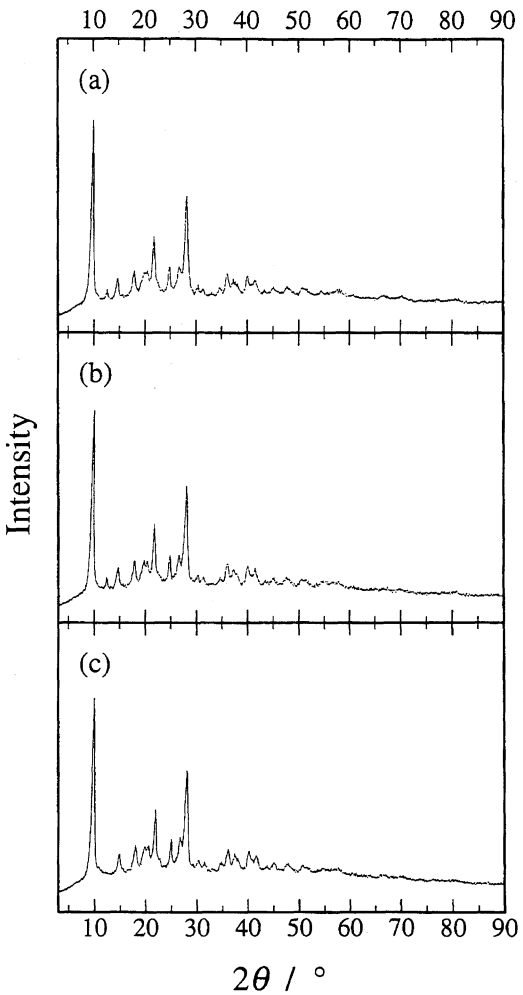

Fig. 8. Powder X-ray diffraction patterns of MnCu(obbz)·$5H_2O$ at (a) 100 K, (b) 200 K, and (c) 300 K.

Looking at Fig. 8 carefully, one can notice that a new small diffraction peak appears around 12.5° below the transition temperature. Although the appearance of this peak may be ascribed to ordering of the crystalline water molecules, single crystal X-ray diffraction analysis is necessary to clarify the detailed crystal structures of the ordered and disordered phases.

This work was partially supported by a Grant-in-Aid for Scientific Research on Priority Areas "Metal-assembled Complexes" (Area No. 401/10149229) from the Ministry of Education, Science, Sports and Culture.

References

1 J. S. Miller, J. C. Calabrese, A. J. Epstein, R. W. Bigelow, J.

H. Zhang, and W. M. Reiff, *J. Chem. Soc., Chem. Commun.*, **1986**, 1026.

2 J. S. Miller, J. C. Calabrese, H. Rommelmann, S. R. Chittipeddi, J. H. Zhang, W. M. Reiff, and A. J. Epstein, *J. Am. Chem. Soc.*, **109**, 769 (1987).

3 J. S. Miller, A. J. Epstein, and W. M. Reiff, *Chem. Rev.*, **88**, 201 (1988).

4 J. S. Miller, A. J. Epstein, and W. M. Reiff, *Science*, **240**, 40 (1988).

5 J. S. Miller, A. J. Epstein, J. C. Calabrese, R. L. Harlow, D. A. Dixon, J. H. Zhang, W. M. Reiff, S. R. Chittipeddi, M. A. Selover, and A. J. Epstein, *J. Am. Chem. Soc.*, **112**, 5496 (1990).

6 Y. Pei, M. Verdaguer, and O. Kahn, *J. Am. Chem. Soc.*, **108**, 7428 (1986).

7 O. Kahn, Y. Pei, M. Verdaguer, J. P. Renard, and J. Sletten, *J. Am. Chem. Soc.*, **110**, 782 (1988).

8 A. Caneschi, D. Gatteschi, and R. Sessoli, *Acc. Chem. Res.*, **22**, 392 (1989).

9 A. Caneschi, D. Gatteschi, J. P. Renard, P. Rey, and R. Sessoli, *Inorg. Chem.*, **28**, 1976 (1989).

10 A. Caneschi, D. Gatteschi, J. P. Renard, P. Rey, and R. Sessoli, *Inorg. Chem.*, **28**, 3314 (1989).

11 F. Lloret, K. Nakatani, Y. Journaux, O. Kahn, Y. Pei, and J. P. Renard, *J. Chem. Soc., Chem. Commun.*, **1988**, 642.

12 K. Nakatani, J. Y. Carriat, Y. Journaux, O. Kahn, F. Lloret, J. P. Renard, Y. Pei, J. Sletten, and M. Verdaguer, *J. Am. Chem. Soc.*, **111**, 5739 (1989).

13 S. Murakawa, T. Wakamatsu, M. Nakano, M. Sorai, and H. Suga, *J. Chem. Thermodyn.*, **19**, 1275 (1987).

14 A. Nishimori, Y. Nagano, and M. Sorai, unpublished.

15 O. Haida, T. Matsuo, H. Suga, and S. Seki, *J. Chem. Thermodyn.*, **6**, 815 (1974).

16 Y. S. Touloukian and T. Makita, "Thermophysical Properties of Matter," ed by Y. S. Touloukian and C. Y. Ho, Plenum, New York– Washington (1970), Vol. 6, p. 102.

17 M. Sorai and S. Seki, *J. Phys. Soc. Jpn.*, **32**, 382 (1972).

18 J. E. Bertie and E. Whalley, *J. Chem. Phys.*, **40**, 1637 (1940).

19 T. A. Scott, Jr., and E. L. Wagner, *J. Chem. Phys.*, **30**, 465 (1959).

20 "Tables of Molecular Vibrational Frequencies Consolidated," ed by T. Shimanouchi, U. S. Government Printing Office, Washington D. C. (1972), Vol. I.

21 K. Kambe, *J. Phys. Soc. Jpn.*, **5**, 48 (1950).

22 T. de Neef, A. J. M. Kuipers, and K. Kopinga, *J. Phys. A*, **7**, L171 (1974).

23 R. H. Sands and W. R. Dunham, *Quart. Rev. Biophys.*, **7**, 443 (1975).

24 L. J. de Jongh and A. R. Miedema, *Adv. Phys.*, **23**, 1 (1974).

25 J. des Cloizeaux and J. J. Pearson, *Phys. Rev.*, **128**, 2131 (1962).

26 F. D. M. Haldane, *Phys. Rev. Lett.*, **50**, 1153 (1983).

27 T. Xiang, *Phys. Rev. B*, **58**, 9142 (1998).

28 K. Asano, Y. Miyazaki, M. Sorai, W. Mori, K. Nakatani, and O. Kahn, manuscript under preparation.